arXiv:1703.02612v1 [cond-mat.mtrl-sci] 7 Mar 2017

Giant and accessible conductivity of charged domain walls in lithium niobate

Christoph S. Werner[1,*], Simon J. Herr[1,*], Karsten Buse[1,2], Boris Sturman[3], Elisabeth Soergel[4], Cina Razzaghi[4], and Ingo Breunig[1,2]

Ferroelectric domain walls are nm-sized interfaces between sections of different allowed values of the spontaneous polarization, the so-called domains. These walls – neutral or charged – can be created, displaced, deleted, and recreated again in ferroelectric materials.[1–3] Owing to the recent progress in the studies of ferroelectrics, they are expected to be functional active elements of the future nano-electronics.[1,4,5] Metallic-like conductivity of charged domain walls (CDWs) in insulating ferroelectrics, predicted in 1970s[6] and detected recently,[7–10] is especially attractive for applications. This important effect is still in its infancy. The electric currents are small, the access to the conductivity is hampered by contact barriers, and stability is low because of sophisticated domain structures and/or proximity of the Curie point. Here, we report on giant and accessible persistent CDW conductivity in lithium niobate (LN) crystals ($LiNbO_3$) – a vital material for photonics.[12] Our results are by far superior to the data known for other materials: Increase of LN conductivity by more than 14 orders of magnitude owing to CDWs, access to the effect via Ohmic and semi-Ohmic contacts, and its high stability for temperatures of up to 70 °C are demonstrated. It is made clear why this big effect was missed earlier[11,25] in LN. Our results demonstrate that strong conductivity of CDWs is available in simple ferroelectric materials, possessing only two allowed orientations of the spontaneous polarization, far from the Curie point. Also, CDW functionalities can be combined with linear and nonlinear optical phenomena.[14,15] Our findings allow new generations of adaptive-optical elements, of electrically controlled integrated-optical chips for quantum photonics, and of advanced LN-semiconductor hybrid optoelectronic devices.

The ferroelectric state can be characterized by the spatial distribution of the spontaneous polarization vector $\boldsymbol{P}_s$. Within a ferroelectric domain $\boldsymbol{P}_s \simeq$ const. Domain walls separate the regions with different allowed polarizations. Often, they are neutral, then the polarization difference $\Delta\boldsymbol{P}_s$ is parallel to the wall plane and the bound polarization charge is zero. Otherwise, the walls are charged and the bound charge is strongly compensated by free charges to ensure the ferroelectric stability.[6,16,17] A simple example of CDW, relevant to our study, is depicted in Fig. 1a. The polarization vectors of the adjacent domains point at the wall (head-to-head CDW), which is tilted by an angle θ to the polarization direction. Here, the bound surface charge is $+2P_s \sin\theta$, and it must be strongly compensated by electrons or negative ions. The electron compensation occurs via the conduction band bending.[6,10,16] It is fast and leads to a metallic-like CDW conductivity because of free movement of electrons along the wall. The width w of CDWs can roughly be estimated as 10 nm, this is one order of magnitude larger than the width of neutral walls.[10,16] For LN polarization $P_s = 70\,\mu\mathrm{C/cm}^2$ and $\theta = 90°$ it gives a huge concentration of electrons, $2P_s/ew \approx 10^{21}$ cm^{-3}, where e is the elementary charge.

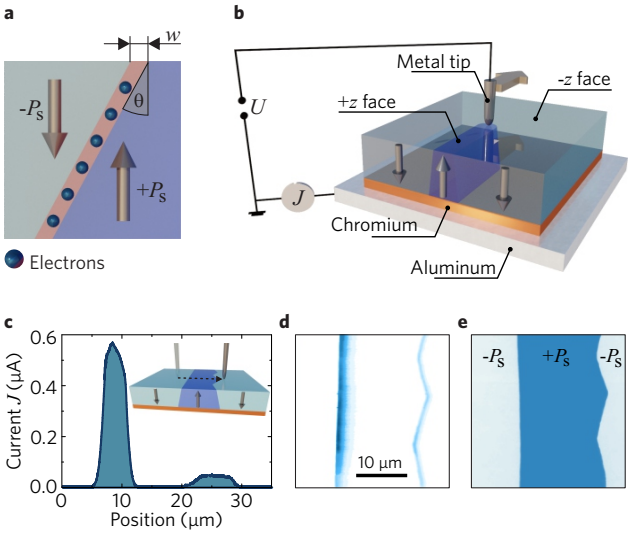

Figure 1: Head-to-head charged domain walls in LN crystals and tip-related experiments on CDW conduction. a, Schematic of a head-to-head CDW in LN crystals; only two opposite directions of $\boldsymbol{P}_s$ are allowed. **b,** Schematic of experimental setup for recording and investigation of CDWs in LN crystals. The vertical arrows show directions of $\boldsymbol{P}_s$. The inverted domain broadens from top to bottom. **c,** The current J versus the tip position about the domain line during a readout experiment at $U = 50$ V. **d,** The spatial distribution $J(x, y)$ corresponding to Fig. 1c obtained with an AFM tip. **e,** The corresponding PFM image identifying the $\pm z$ domains.

*These authors contributed equally to this work.
[1]Department of Microsystems Engineering - IMTEK, University of Freiburg, Georges-Köhler-Allee 102, 79110 Freiburg, Germany.
[2]Fraunhofer Institute for Physical Measurement Techniques IPM, Heidenhofstraße 8, 79110 Freiburg, Germany.
[3]Institute for Automation and Electrometry of Russian Academy of Science, 630090 Novosibirsk, Russia.
[4]Institute of Physics, University of Bonn, Wegelerstraße 8, 53115 Bonn, Germany.

CDWs and their elevated conductivity were occasionally observed in the past.[19,20] During the last decade, they were well documented in many materials including $BiFeO_3$,[21] $BaTiO_3$,[9,22] $ErMnO_3$,[23] and h-$HoMnO_3$.[24] High-resolution transmission-electron and atomic-force microscopies were extensively used. The most advanced data on the CDW conductivity has been presented so far for $BaTiO_3$ single crystals. An enhancement factor $\sim 10^9$, as compared to the conductivity of the bulk, was obtained for 45° head-to-head walls. The data reported suffer from bad stability and big contact barriers leading to pronounced non-Ohmic current-voltage characteristics. Experiments with LN crystals have shown either transient conductivity[25] or steady conductivity just in the presence of super-band-gap illumination.[11]

Our choice of LN crystals for domain-wall-electronic studies has strong grounds. This robust and cheap wide-band-gap material ($E_g \simeq 4$ eV) is extremely useful for numerous optical applications.[12,14] As a ferroelectric, it has a very high Curie temperature, $T_C \approx 1200\,^\circ$C, and only two allowed (opposite) values of $\boldsymbol{P}_s$.[28] Field-assisted domain engineering is a well-developed area because of the quasi-phase-matching applications.[12,26,27] The dark conductivity of LN crystals is extremely low.[28]

In our experiments, we used mainly 300-μm-thick z-cut samples of congruent LN doped with 5 mol.% MgO. The data presented in this article correspond to this material. However, similar data were obtained with near-stoichiometric LN. In order to produce domain structures in originally single-domain crystals, we employed the calligraphic domain writing.[27] It is shown schematically in Fig. 1b. The bottom $+z$ face was coated with a 0.5-μm-thick Cr electrode and then glued with conductive paste to a heatable aluminum mount. The temperature T can be controlled on the 0.1 °C level within the range $(20-150)\,^\circ$C. As the top electrode we use a tungsten-carbide needle with μm-sized tip radius. During the domain-inversion procedure, the tip is moving slowly along the x direction producing a domain line which is typically as long as 1 mm. The applied voltage U is kept such that the poling current $J \simeq 30$ nA. Subsequent etching of the sample shows that the domain size on the $+z$ face of the untreated crystal noticeably and reproducibly exceeds the size on its $-z$ face. Thus, the domain walls are slightly tilted, and they must be positively charged. The tilt angle can be estimated as $\theta \approx 1^\circ$. Remarkably, the total charge flowed through the sample during the domain-inversion procedure exceeds the net polarization charge by orders of magnitude. This is an indication of CDW conductivity. The major experimental differences compared to previous work are the use of room temperature poling and the avoidance of after-poling heat treatment.

In the first series of experiments on the prepared domain structure, a virgin μm-sized tip is moving slowly across the domain line, as shown in the inset of Fig. 1c. The voltage is decreased to 50 V to reduce the applied field far below the coercive field ($E_c \gtrsim 3$ kV/mm) and hence to avoid any field effect on the domain structure. The current is nonzero only when crossing the left and right domain borders; this proves that CDWs are responsible for the conduction. The value $J_{\max} \simeq 0.55\,\mu$A is very high for tip-related experiments. The relative asymmetry between the left and right borders in Fig. 1c is occasional – it varies when crossing different sections of the domain line. Employment of a conductive AFM tip of about 50 nm radius has allowed us to map the current distribution in the same area, see Fig. 1d. Within the actual spatial resolution, the conductivity is strongly localized at the left CDW. Relative smallness of the current near the right wall correlates with its zigzag structure. The PFM image of the same area, see Fig. 1e, reproduces the straight left border of the domain and its zigzag right border.

Next, we kept our μm-sized tip at the point of maximum of $J(y)$ and measured the current-voltage characteristics. The corresponding result is presented in Fig. 2.

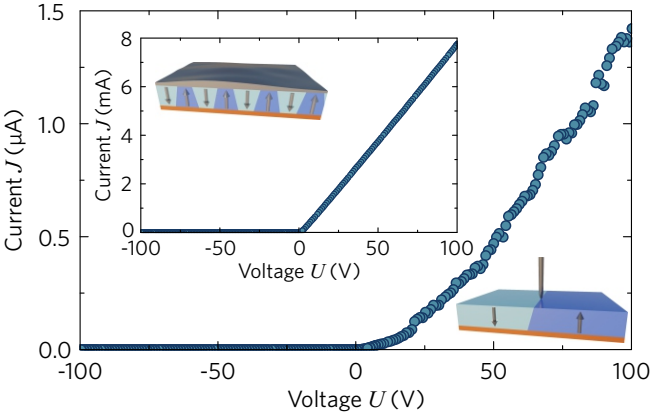

Figure 2: Diode-like current-voltage dependence at the point of maximum of $J(y)$ for a single domain line. The inset corresponds to an array of 732 lines covered with a silver-paste top electrode. The tilts of the walls are exaggerated.

A pronounced diode-like dependence of $J(U)$ is clearly seen. For $U < 0$ the current is practically absent, while for $U \gtrsim 30$ V we have an almost quasi-Ohmic behavior. While the Schottky-like $J(U)$ characteristic is typical for a tip experiment, the quasi-Ohmic behavior is rather special. The above $J(U)$ measurement has then been advanced. Instead of a single domain line we have recorded an array of 732 parallel 1-mm-long domain lines. After that, the top face was covered with conductive silver paste. Application of voltage leads here to a strikingly regular semi-Ohmic $J(U)$ characteristic, see the inset in Fig. 2. For $U > 0$, this characteristic is practically linear showing the absence of electrode barriers. The values of the current approach here 0.01 A.

The above data allow us to evaluate reliably the CDW conductivity. To make so, we calculate the total resistance of the system $R = U/J$ under the assumption of Ohmic contacts. Since the problem is two-dimensional, we have generally for a single wall: $R_1 = \rho_s F$, where $\rho_s = (\sigma w)^{-1}$, ρ_s is the specific surface CDW resistivity, σ is the average conductivity inside the wall, and F is a dimensionless factor determined by the geometry of the contacts.[30] Let L and a be the domain-line length and the electrode length along the wall, respectively. For a continuous top electrode we have $a \simeq L \gg d$. Here, the stream lines of the current are parallel to each other and, by analogy with the plane capacitor, we have $F \simeq d/L$. For N parallel-connected CDWs we have $R \simeq \rho_s d/NL$. Setting $d = 300\,\mu$m, $L = 1$ mm, $N = 732$, and estimating V/J from

the inset of Fig. 2, we obtain $\rho_s \simeq 3.1 \times 10^7\,\Omega$. In the tip-electrode case, the stream lines of the current are expanding in the wall plane with the distance from the top electrode. Numerical simulations give here $F \simeq 0.72\,\lg(5d/a)$. This logarithmic dependence on d/a is fairly weak. Setting $a = 2\,\mu$m, which is not far from the tip diameter, and estimating $R_1 = U/J$ from Fig. 2, we obtain $\rho_s \approx 3.5\times10^7\,\Omega$. The consistency of the two independent estimates, obtained for different contacts and geometries, is striking. Setting next $w = 10$ nm, we obtain for the bulk CDW conductivity: $\sigma \approx 0.03\ (\Omega\,\mathrm{cm})^{-1}$. This value exceeds the dark conductivity of LN crystals[28] by at least 14 orders of magnitude. Finally, using the relation $\sigma = e\mu_e n$ and setting for the electron drift mobility $\mu_e \lesssim 0.1$ cm^2/Vs, we obtain for the concentration of compensating electrons: $n \gtrsim 1.8 \times 10^{18}$ cm^{-3}. This is in fair agreement with the estimate $n \approx 2P_s\theta/ew$ for $\theta \approx 1^\circ$.

Our experimental efforts are directed next to elucidate the origin of the contact barriers and to get access to the CDW conductivity through fully Ohmic contacts. To accomplish this challenging task, we have recorded an array of sixteen 13-mm-long domain lines. Then the central part of the bottom Cr electrode has been etched away, and two spatially separated droplets of conductive paste are used as two top electrodes, see Fig. 3a.

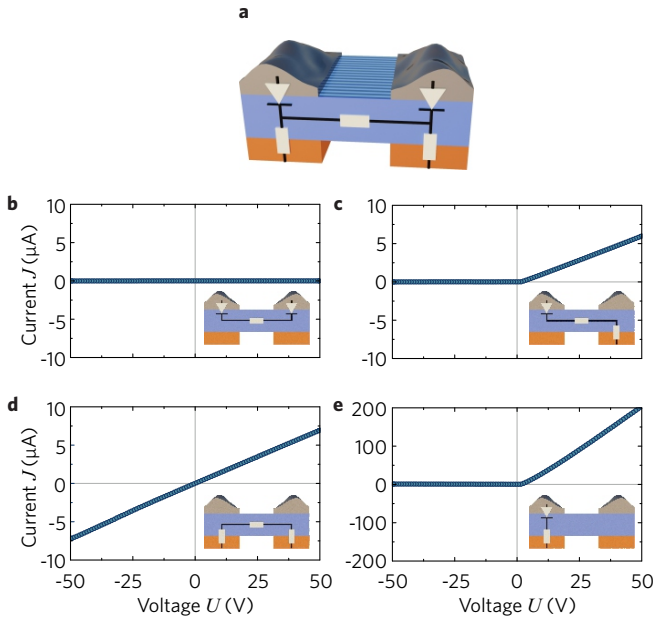

Figure 3: Origin of contact barriers and Ohmic access to CDW conductivity. a, Geometry of four-electrode configuration and an equivalent electric scheme. **b,** Top-Top connection: zero current. **c,** Top-left-Bottom-right connection: semi-Ohmic behavior. **d,** Bottom-Bottom connection: fully Ohmic behavior. **e,** Top-left-Bottom-left connection: semi-Ohmic behavior.

Zero current was observed when the voltage was applied between two top electrodes, see Fig. 3b. This shows unambiguously that the top electrodes act as almost perfect top-bottom diodes. Applying voltage between the left-top and right-bottom electrodes or between right-top and left-bottom electrodes (Figs. 3c and 3e) returns us to the known semi-Ohmic behavior. Lastly, applying voltage between two bottom electrodes, Fig. 3d, we obtain the fully Ohmic behavior. This indicates that the bottom electrode is Ohmic. An equivalent electrical scheme for our four-electrode configuration is presented in Fig. 3a. It is worthy of mentioning that removal of the original Cr electrode with subsequent re-contacting leads to a pronounced non-Ohmic behavior. This observation excludes, in particular, the possibility of leakage currents between the two bottom Cr electrodes.

The effect of heating on the CDW conductivity is an important issue. For temperature measurements, we used a sample with thirty 1-mm-long domain lines and a silver-paste top electrode. Up to $T = 70\,^\circ$C, the conductivity shows no signs of temporal degradation within the period of about one day. For example, observation of $J(t)$ during 35 hours at $T = 30\,^\circ$ indicates that the current fluctuates around an average value within only 1%, see Fig. 4a.

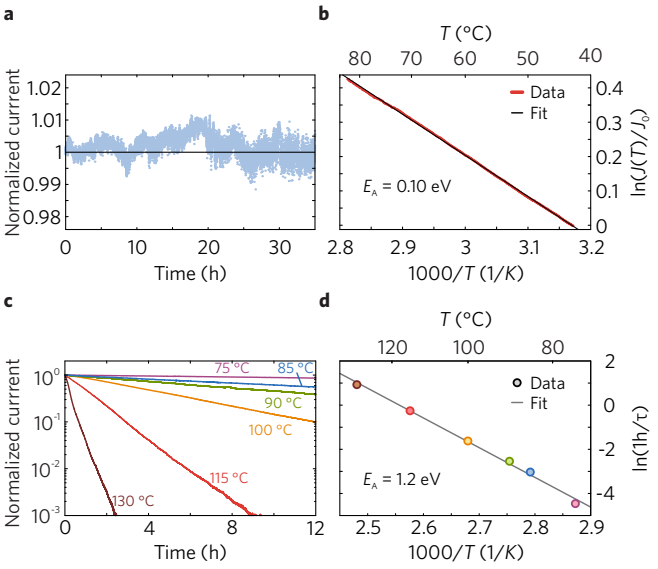

Figure 4: Results of temperature-related measurements. a, Temporal dependence $J(t)$ at $30\,^\circ$C. **b,** Arrhenius plot of steady-state value of $J(T)$ for the temperature range $(40-85)\,^\circ$C. **c,** Time decay of J for $T = 75$, 85, 90, 100, 115, and $130\,^\circ$C. **d,** Arrhenius plot of the decay rate τ^{-1} for $T = (72-135)\,^\circ$C.

This contrasts with much stronger fluctuations of $J(t)$ in $BaTiO_3$ and $BiFeO_3$. For $T \leq 70\,^\circ$, the current increases with temperature according to an Arrhenius law with the activation energy $E_A = (0.10 \pm 0.01)$ eV, see Fig. 4b. This temperature-activation dependence is the signature of hopping electron conductivity. For temperatures $T > 70\,^\circ$C and on long time scales, the current decays exponentially in time, $J(t)/J(0) = \exp(-t/\tau)$, see Fig. 4c. The higher T, the faster is the decay. Once the conductivity has vanished by heating, it cannot be recovered. The decay rate $\tau^{-1}(T)$ also obeys an Arrhenius law with the activation energy $E_A = (1.2 \pm 0.1)$ eV, see Fig. 4d. This value strongly indicates that migration of some ions is responsible for the high-temperature decay of the

CDW conductivity.

Looking forward, it will be relevant to fully elucidate the effect reported here, in particular with the aim to control all parameters: In-depth understanding is needed how the inhomogeneous field employed for the calligraphic poling plus defects that pin the domain walls influence the key outcome, the tilt of the domain walls. However, already now it is clear that this effect can pave the way to novel integrated electronic-optical devices: Calligraphically written charged domain walls can serve in a z-cut waver as electrodes to access the electro-optical coefficient r_{22}, providing electrically controlled local phase modulation. Patterning the wafer and contacting the electrodes with nanometer-thin Ag wires allows the design of freely programmable optical phase plates. Our findings will be also of use for integrated reconfigurable quantum-optical devices providing, e.g., correlated photons from electro-optically tunable difference-frequency generation. Flip-bonding a Si chip onto LN samples with tailored conducting domain walls allows to apply freely designed 2D-structured electrical fields to LN crystals, stimulating the field of LN-semiconductor hybrid chips.

[1] Catalan, G., Seidel, J., Ramesh, R., & Scott, J., F. Domain wall electronics, *Reviews of Modern Physics* **84**, 119-156 (2012).

[2] Bednyakov, P. S., Sluka, T., Tagantsev, A. K., Damjanovic, D. & Setter, N. Formation of charged ferroelectric domain walls with controlled periodicity. *Sci. Rep.* **5**, 15819 (2015).

[3] Feigl, L., Sluka, T., McGilly, L. J., Crassous, A., Sandu, C. S. & Setter, N. Controlled creation and displacement of charged domain walls in ferroelectric thin films. *Sci. Rep.* **6**, 31323 (2016).

[4] Seidel, J. Domain walls as nanoscale functional elements. *J. Phys. Chem. Lett.* **3**, 2905-2909 (2012).

[5] Vasudevan, R. K. *et al.* Domain wall conduction and polarization-mediated transport in ferroelectrics. *Adv. Funct. Mater.* **23**, 2592-2616 (2013).

[6] Vul, B. M., Guro, G. M. & Ivanchik, I. I. Encountering domains in ferroelectrics. *Ferroelectrics* **6**, 29-31 (1973).

[7] Maksymovych, P. *et al.* Tunable metallic conductance in ferroelectric nanodomains. *Nano Lett.* **12**, 209-2013 (2012).

[8] Vasudevan, R. K. *et al*, Domain wall geometry controls conduction in ferroelectrics. *Nano. Lett.* **12**, 5524-5531 (2012).

[9] Sluka, T., Tagantsev, A. K., Bednyakov, P. & Setter, N. Free-electron gas at charge domain walls in insulating $BaTiO_3$. *Nat. Commun.* **4**, 1808 (2013).

[10] Sluka, T., Bednyakov, P., Yudin, P., Crassous, A., & Tagantsev, A. Charged domain walls in ferroelectrics, chapter in Topological structures in ferroic materials - domain walls, vortices, and skyrmions. Springer Series in Material Science **228**, 103-138 (2016).

[11] Schröder, M. *at al.* Conducting domain walls in lithium niobate single crystals. *Adv. Funct. Mater.* **22**, 3936-3944 (2012).

[12] Arizmendi, L. Photonic applications of lithium niobate crystals. *Phys. Stat. Sol.* **201**, 253283 (2004).

[13] Shur, V. Ya., Baturin, I. S., Akhmatkhanov, A. R., Chezganov, D. S. & Esin, A. A. Time-dependent conduction current in lithium niobate crystals with charged domain walls. *Appl. Phys. Lett.* **103**, 102905 (2013).

[14] Dunn, M. H., & Ebrahimzadeh, M. Parametric generation of tunable light from continuous-wave to femtosecond pulses. *Science* **286**, 1513-1517 (1999).

[15] Weigel, P. O. *et al.* Lightwave circuits in lithium niobate through hybrid waveguides with silicon photonics. *Sci. Rep.* **6**, 22301 (2016).

[16] Guriev, M. Y., Tagantsev, A. K. & Setter, N. Head-to-head and tail-to-tail 180° domain walls in an isolated ferroelectric. *Phys. Rev. B* **83**, 184101 (2011).

[17] Zuo, Y. Genenko, Y. A. & Xu, B.-X. Charge compensation of head-to-head and tail-to-tail domain walls in barium titanate and its influence on conductivity. *J. Appl. Phys.* **116**, 044109 (2014).

[18] Eliseev, E. A., Morozovska, A. N., Svechnikov, G. S., Gopalan, V., & Shur, V. Ya. Staic conductivity of charged domain walls in uniaxial ferroelectric semiconductors. *Phys. Rev. B* **83**, 235313 (2011).

[19] Grekov, A. A., Adonin, A. A., & Protsenko, N. P. Encountering domains in SbSI. *Ferroelectrics* **13**, 483-485 (1976).

[20] Seidel, J. *et al.* Conduction at domain walls in oxide multiferroics. *Nat. Mat.* **8**, 229-234 (2009).

[21] Crassous, A., Sluka, T., Tagantsev, A., & Setter, N. Polarization charge as a reconfigurable quasi-dopant in ferroelectric thin films, *Nat. Nanotechnol.* **10**, 614-618 (2015).

[22] Bednyakov, P. Sluka, T., Tagantsev, A., Damjanovic, D. & Setter, N. Free-carrier-compensated charged domain walls produced with super-bandgap illumination in insulating ferroelectrics. *Adv. Mater.* DOI: 10.1002/adma.201602874 (2016).

[23] Meier, D. *et al.* Anisotropic conductance at improper ferroelectricdomain walls. *Nat Mat.* **11**, 284-288 (2012).

[24] Wu, W., Horibe, Y., Lee, N., Cheong, S.-W. & Guest, J. R. Conduction of topologically protected charged ferroelectric domain walls. *Phys. Rev. Lett.* **108**, 077203 (2012).

[25] Shur, V. Ya., Baturin, I. S., Akhmatkhanov, A. R., Chezganov, D. S. & Esin, A. A. Time-dependent conduction current in lithium niobate crystals with charged domain walls. *Appl. Phys. Lett.* **103**, 102905 (2013).

[26] Terabe, K. *et al.* Microscale to nanoscale ferroelectric domain and surface engineering of a near-stoichiometric $LiNbO_3$ crystal. *Appl. Phys. Lett.* **82**, 433435 (2003).

[27] Mohageg, M. *et al.* Calligraphic poling of lithium niobate. *Opt. Express* **13**, 3408-3419 (2005).

[28] Properties of Lithium Niobate, K. K. Wong, ed. (2002).

[29] Li, L. *et al.* Atomic scale structure changes induced by charged domain walls in ferroelectric materials. *Nano. Lett.* **13**, 5218-5223 (2013).

[30] Smythe, W. R. *Static and Dynamic Electricity.* (McGraw-Hill, 1950).